Exceptionally bright TeV flares from the binary LS I +61° 303

Anna OFdB[1], Andy Smith[2], VERITAS Collaboration[3]

ABSTRACT

The TeV binary system LS I +61° 303 is known for its regular, although not entirely understood, non-thermal emission pattern which traces the orbital period of the compact object in its 26.5 day orbit around its Be star companion. When active in the TeV regime, the system typically presents elevated emission around apastron passage with flux levels in the 5 – 15 % Crab Nebula range (> 300 GeV). In this article, VERITAS observations of LS I +61° 303 taken in late 2014 are presented, during which bright TeV flares around apastron at flux levels peaking above 30% of the Crab Nebula flux were detected. This is the brightest such activity from this source ever seen in the TeV regime. The strong outbursts have rise and fall times of less than a day. The short timescale of the flares, in conjunction with the observation of 10 TeV photons from LS I +61° 303 during the flares, provides constraints on the nature and efficiency of the accelerating mechanism in the source.

Subject headings:

1. Introduction

The current generation of imaging atmospheric-Cherenkov telescopes (IACTs) has opened up the study of those high-mass X-ray binary (HMXB) systems which exhibit TeV emission on various timescales. The class of TeV binaries is quite sparse, consisting of only a handful of sources: LS 5039 (Aharonian et al. 2005b), PSR B1259-63 (Aharonian et al. 2005a), LS I +61° 303 (Albert et al. 2006), HESS J0632+057 (Acciari et al. 2009), and the newest member of the class 1FGL J1018.6-5856 (Abramowski et al. 2015). Of these, only the compact object of PSR B1259-63 has been firmly identified as a pulsar; there is still a large degree of ambiguity concerning the nature of the compact object within the other systems. Consequently, the fundamental setup that produces the TeV emission along with its characteristic variability on the timescale of one orbital period.

The orbital periods of HMXBs vary from several days (LS 5039) to several years (PSR B1259-63). As the TeV emission varies strongly as function of the orbital phase, the various sources may only have short windows during which they can be studied in the TeV regime. Of the TeV binaries, LS I +61° 303 is the only known source in the Northern Hemisphere that has a short enough orbital period (26.5 days) to allow for regular study with TeV instruments.

Located at a distance of ~2 kpc (Frail & Hjellming 1991), LS I +61° 303 is composed of a B0 Ve star and a compact object (Hutchings & Crampton 1981; Casares et al. 2005). The observed emission is variable and modulated with a period of $P \approx 26.5$ days, believed to be associated with the orbital structure of the binary system (Albert et al. 2006; Esposito et al. 2007; Acciari et al. 2008; Abdo et al. 2009; Li et al. 2012; Massi et al. 2015). Radial velocity measurements show the orbit to be elliptical $e = 0.537 \pm 0.034$, with periastron occurring around phase $\phi = 0.275$, apastron at $\phi = 0.775$, superior conjunction at $\phi = 1.081$ and inferior conjunction at $\phi = 0.313$ (Aragona et al. 2009). The periastron distance between the star and the compact object is estimated at 2.84×10^{12} cm (0.19 AU) and the apastron distance at 9.57×10^{12} cm (0.64 AU) (Dubus 2013). However, the inclination of the system is not exactly

[1]Germany

[2]America

[3]Everywhere

known (it is expected to lie in the range $10° - 60°$ according to Dubus (2013)), leading to some uncertainty of the orbital parameters.

In this work, we present the results of the VERITAS campaign on LS I +61° 303 in the Fall of 2014. During this time, VERITAS observed historically bright flares from LS I +61° 303 around apastron, with the source exhibiting flux levels a factor of $2-3$ times higher than ever previously observed.

2. Observations

The VERITAS IACT array, located at the base of Mt. Hopkins, AZ (1.3 km a.s.l., 31°40' N, 110°57' W) consists of four 12 m diameter Davies-Cotton design optical telescopes. VERITAS is sensitive to photons with energies from 85 GeV to 30 TeV and has the ability to detect a 1 % Crab Nebula source in approximately 25 hours[1]. For a full description of the hardware components and analysis methods utilized by VERITAS, see Holder et al. (2008); Kieda, D. (2013); Acciari et al. (2008), and references therein.

In the 2014 season, VERITAS observations of LS I +61° 303 were taken from October 16 (MJD 56946) to December 12 (MJD 57003), obtaining a total of 24.7 hours of quality selected livetime. These observations covered three separate orbital periods, sampling the orbital phase regions of $\phi = 0.5 - 0.2$ (see Figure 1 and Table 1). Over the entire set of observations, a total of 449 excess events above an energy threshold of 300 GeV were detected above background, equivalent to a statistical significance of 21 standard deviations above background (21σ, calculated using Equation 17 of Li & Ma (1983)).

During the first orbit observed (in October), the source presented the largest of its flares (hereafter "F1"), beginning on 2014 October 17 (MJD 56947, $\phi = 0.55$) with emission reaching a peak of $(31.9 \pm 3.4) \times 10^{-12}$ photons cm^{-2} s^{-1} on October 18 (MJD 56948). This flare reached a peak flux of approximately 30% of the Crab Nebula flux in the same energy range, representing the largest flux ever detected from the source. Unfortunately, observations were limited by poor weather conditions for the following two nights and only recommenced on October 20 (MJD 56950), by which time the flux from the source had already decreased. During the second orbital passage in November, VERITAS detected another period of elevated flux ("F2") from the source at similar orbital phases ($\phi = 0.5 - 0.6$) with peak emission of $(20.2 \pm 2.2) \times 10^{-12}$ photons cm^{-2} s^{-1} on November 14 (MJD 56975).

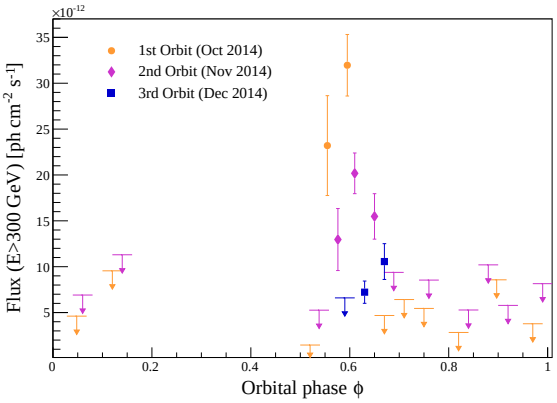

Fig. 1.— Light curve of LS I +61° 303 during the 2014 observation season in nightly bins. The data are for the first orbit (October) are shown with orange circles, the data for the second orbit are shown with purple diamonds, and the data for the third orbit are shown with blue squares. Flux upper limits at the 99% confidence level (using the unbounded approach of Rolke et al. (2005)) are shown for points with $< 3\,\sigma$ significance and are represented by arrows.

The rise and fall times of the flares were determined by fitting Equation 7 of Abdo et al. (2010) to the light curve of each orbit and fixing t_0 to the MJD of the observed peak. The fit to the first orbit is not very good, with a fit probability of 3×10^{-7}. Nevertheless, the rise and fall times of F1 are found to be 0.39 ± 0.07 days and 0.37 ± 0.23 days, respectively. The second orbit is well fit by this function, with a fit probability of 1×10^{-1}, possibly due to the better data sampling throughout this flare. The rise and fall times of F2 are thus found to be 0.65 ± 0.13 days and 0.83 ± 0.12 days, respectively. A piecewise defined exponential function was also fit to F1 and F2, but resulted in a very poor fit probability for both flares.

[1] http://veritas.sao.arizona.edu/about-veritas-mainmenu-81/veritas-specifications-mainmenu-111

TABLE 1
VERITAS OBSERVATIONS OF LS I +61° 303 IN 2014

Date observed [MJD]	Orbital phase (ϕ)	Flux($> 300\,\mathrm{GeV}$) [$\times 10^{-11}$ cm^{-2} s^{-1}]
56946.3	0.52	<0.15
56947.3	0.55	2.32 ± 0.54
56948.3	0.60	3.20 ± 0.34
56950.0	0.67	<0.47
56951.0	0.71	<0.64
56952.0	0.75	<0.55
56954.0	0.82	<0.28
56956.0	0.90	<0.86
56958.0	0.97	<0.38
56960.0	0.05	<0.46
56962.0	0.12	<0.96
56973.0	0.54	<0.53
56974.0	0.58	1.30 ± 0.34
56975.0	0.61	2.02 ± 0.22
56976.0	0.65	1.55 ± 0.25
56977.0	0.69	<0.94
56979.0	0.76	<0.85
56981.0	0.84	<0.53
56982.0	0.88	<1.02
56983.0	0.92	<0.58
56985.0	0.99	<0.82
56987.0	0.06	<0.69
56989.0	0.14	<1.13
57001.0	0.59	<0.66
57002.0	0.63	0.72 ± 0.12
57003.0	0.67	1.06 ± 0.20

Variability on a nightly timescale was tested using the method described in Aliu et al. (2013). Similar to their findings for this source, of a hint of nightly variability at a significance level of ~$3\,\sigma$ post trials was found in F1.

Follow-up observations conducted by VERITAS during the next month (2014 December 10 – 12) covered the orbital phases of $\phi = 0.59 - 0.67$ and detected the source at a lower flux level, reaching only $(7.2 \pm 1.2) \times 10^{-12}$ photons cm^{-2} s^{-1} around the orbital phase at which the flares were detected in the previous orbits. The observations during this month seem to exclude the type of peaked flaring behavior seen at the same phase range in the previous two orbital cycles, perhaps indicating some orbit-to-orbit variations in the source.

The average differential energy spectrum from all observations of LS I +61° 303 during the 2014 observing season is well fit with a power law of the form

$$\frac{dN}{dE} = N_0 \left(\frac{E}{1\,\mathrm{TeV}} \right)^{\Gamma}. \qquad (1)$$

The measured parameters are consistent with past observations, with $N_0^{\mathrm{avg}} = (1.7 \pm 0.7_{\mathrm{stat}} \pm 0.9_{\mathrm{sys}}) \times 10^{-12}$ cm^{-2} s^{-1} TeV^{-1} and $\Gamma^{\mathrm{avg}} = -2.35 \pm 0.32_{\mathrm{stat}} \pm 0.3_{\mathrm{sys}}$ in the 0.3 – 20 TeV range. Differential energy spectra are also extracted from F1 (October 17 – 18) and F2 (November 13 – 15) and show a similar spectral shape, albeit with a higher normalization constant. The fit to the spectrum of F1 gives $N_0^{\mathrm{F1}} = (8.6 \pm 1.0_{\mathrm{stat}} \pm 4.3_{\mathrm{sys}}) \times 10^{-12}$ cm^{-2} s^{-1} TeV^{-1} and $\Gamma^{\mathrm{F1}} = -2.24 \pm 0.12_{\mathrm{stat}} \pm 0.3_{\mathrm{sys}}$ and the spectrum of F2 is described by $N_0^{\mathrm{F2}} = (4.8 \pm 0.4_{\mathrm{stat}} \pm 2.4_{\mathrm{sys}}) \times 10^{-12}$ cm^{-2} s^{-1} TeV^{-1} and $\Gamma^{\mathrm{F2}} = -2.36 \pm 0.12_{\mathrm{stat}} \pm 0.3_{\mathrm{sys}}$. The average and flare spectra are shown in Figure 2 along with previous spectral measurements for comparison. An uncertainty in the energy scale of 15 – 25% results in a systematic uncertainty of ~50% on the flux normalization and ~40% on the integral flux, assuming a spectral index of -2.5. The systematic uncertainty on the spectral index is estimated at ~0.3, accounting for uncertainties on the collection efficiency, sky brightness, analysis cuts, and simulation model.

The highest energy gamma ray observed during these observations was detected during the peak night of F1 with an energy of ~10 TeV (using a conservative estimate of the energy). There are no background events with an energy 4 TeV on this night, so it is assumed that the contribution of the background at ~10 TeV is negligible.

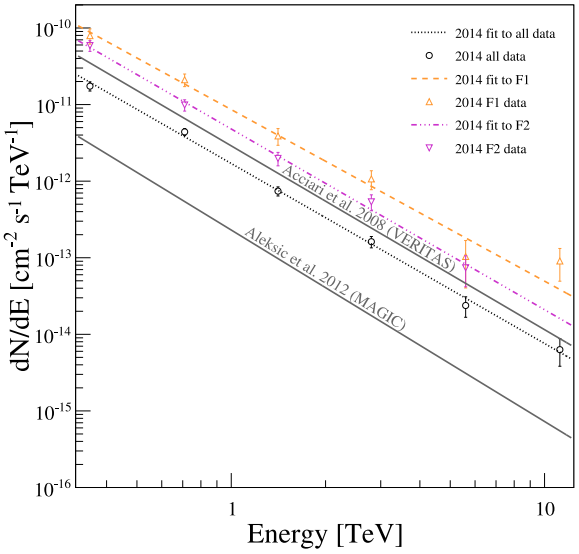

Fig. 2.— Average and flare differential energy spectra of LS I +61° 303 from the VERITAS 2014 observations, shown in comparison with the average spectra from Acciari et al. (2008) and Aleksic et al. (2012).

During these observations, the source was also monitored by the *Fermi*-LAT (0.1 – 300 GeV), the *Swift*-XRT (0.2 – 10 keV), and both the RATAN and AMI radio instruments (4/6 – 15 GHz). In addition, H-alpha monitoring of the system took place at the Ritter Observatory in Toledo, Ohio (USA). After F2 was detected by VERITAS, an ATel (Holder 2015) was released, notifying the astronomical community of the historic flux levels and triggering more intense observations by multiwavelength partners, as well as additional observations with the MAGIC TeV observatory. The results of this campaign are under analysis and will be presented in an upcoming publication.

3. Discussion and Conclusion

The nature of the compact object in LS I +61° 303 is not firmly established, forcing emission mechanisms proposed for the system to cover a range of possibilities. These mechanisms

breakdown into two main categories: microquasar (μQ) and pulsar binary (PB). In the μQ scenario, non-thermal particle acceleration processes occur in the jet of an accreting compact object (Massi et al. 2001; Massi & Jaron 2013; Massi et al. 2015), whereas the binary pulsar scenario utilizes the presence of a shocked wind in which particle acceleration is the result of the interaction between the stellar and the pulsar winds (Dhawan et al. 2006). While some versions of both models utilize a hadronic primary population, the vast majority of both model types employ leptonic origins for the observed non-thermal emission.

In a leptonic scenario, the TeV emission is the result of inverse-Compton (IC) scattering of electrons accelerated in the jet (μQ) or at the shock front (BP). Regardless of the primary mechanism for generation, Khangulyan et al. (2008) provides the means to calculate model-independent limits on the magnetic field strength and the efficiency of the accelerator within an IC scenario. It is assumed that the gamma rays are produced in the system by the IC scattering of TeV electrons on stellar photons. Given the temperature $T = 2.25 \times 10^4\,\mathrm{K}$ (Dubus 2013) of the Be star in LS I +61° 303, the average energy of the stellar photons is $3kT \approx 6\,\mathrm{eV}$, and the IC scattering will take place in the deep Klein–Nishina regime, in which all of the electron energy is transferred to the scattered photons. Thus, the presence of ~10 TeV photons requires ~10 TeV electrons in the emitter, as well as forcing the acceleration time to be less than the cooling time. Following the calculations of Khangulyan et al. (2008), the acceleration timescale of the electrons can be expressed as

$$t_{\mathrm{acc}} = \eta_{\mathrm{acc}} r_{\mathrm{L}} c^{-1} \approx 0.1 \eta_{\mathrm{acc}} E_{\mathrm{TeV}} B_{\mathrm{G}}^{-1}\,\mathrm{s}, \quad (2)$$

where r_{L} is the Larmor radius of the electron, E_{TeV} is the energy of the electron in units of TeV, B_{G} is the magnetic field strength in units of Gauss, and $\eta_{\mathrm{acc}} > 1$ is a parameter describing the efficiency of the accelerator (in general $\eta_{\mathrm{acc}} \gg 1$). The characteristic cooling time of electrons in the Klein–Nishina regime is given by

$$t_{\mathrm{KN}} \approx 10^3 d_{13}^2 E_{\mathrm{TeV}}^{0.7}\,\mathrm{s}, \quad (3)$$

where d_{13} is the distance between the emitter and the optical star in units of 10^{13} cm, and the synchrotron cooling time is

$$t_{\mathrm{sy}} \approx 4 \times 10^2 B_{\mathrm{G}}^{-2} E_{\mathrm{TeV}}^{-1}\,\mathrm{s}. \quad (4)$$

Hard gamma-ray spectral indices (from -2 to -2.5) require that $t_{\mathrm{KN}} < t_{\mathrm{sy}}$ due to the fact that IC losses in the Klein-Nishina regime allow for the hard electron spectra (harder than -2) necessary to produce such gamma-ray indices. Thus, the magnetic field in the emitter is constrained by the relation

$$B < 0.6 d_{13}^{-1} E_{\mathrm{TeV}}^{-0.85}\ \mathrm{G}. \quad (5)$$

Using $E_{\mathrm{TeV}} = 10$, as measured during F1, gives values of $B \lesssim 0.3\,\mathrm{G}$ at periastron and $B \lesssim 0.1\,\mathrm{G}$ at apastron, assuming that the emitter is located close to the compact object.

As the cooling time is dominated by t_{KN}, the requirement that the acceleration time is less than the cooling time yields the relation $t_{\mathrm{acc}} < t_{\mathrm{KN}}$ which gives

$$B > 10^{-4} d_{13}^{-2} E_{\mathrm{TeV}}^{0.3} \eta_{\mathrm{acc}}\ \mathrm{G}. \quad (6)$$

This gives values of $B \gtrsim (2.5 \times 10^{-3}) \eta_{\mathrm{acc}}$ G at periastron and $B \gtrsim (2.2 \times 10^{-4}) \eta_{\mathrm{acc}}$ G at apastron, if the emitter is close to the compact object. Using the lower and upper limits on the magnetic field strength, an upper limit can be placed on the acceleration efficiency of $\eta_{\mathrm{acc}} \lesssim 120$ at periastron and $\eta_{\mathrm{acc}} \lesssim 454$ at apastron.

Figure 3 shows the acceleration time t_{acc} as a function of the magnetic field strength B for different values of the accelerator efficiency η_{acc}, assuming an electron energy of 10 TeV. The upper limits on the magnetic field strength at periastron and apastron, which are independent of η_{acc}, are marked. Two areas of the plot are shaded to indicate the allowed regions of the parameter space, corresponding to $t_{\mathrm{acc}} < 1\,\mathrm{day}$, $B < 0.3\,\mathrm{G}$, and $\eta_{\mathrm{acc}} < 120$ at periastron and $t_{\mathrm{acc}} < 1\,\mathrm{day}$, $B < 0.1\,\mathrm{G}$, and $\eta_{\mathrm{acc}} < 454$ at apastron.

The constraints are strongly dependent on the location of the emitter, which has been assumed to be coincident with the compact object in order to derive these limits.

Paredes-Fortuny et al. (2015) present a general pulsar wind shock scenario with an inhomogeneous stellar wind in which the Be star disc is disrupted and fragments, and these fragments fall into the shock region, pushing it closer to the pulsar. The

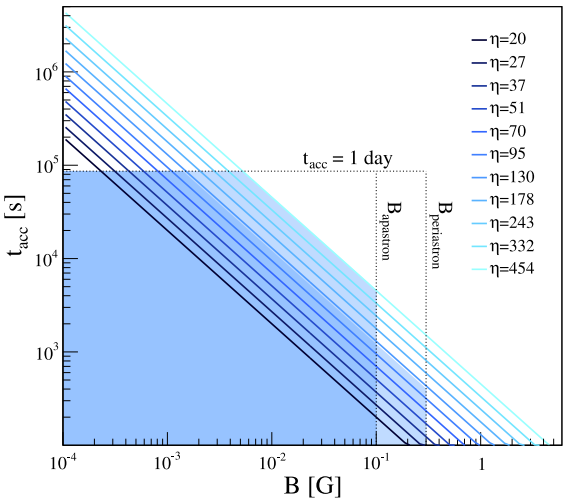

Fig. 3.— Acceleration time $t_{\rm acc}$ as a function of the magnetic field strength B for different values of the accelerator efficiency $\eta_{\rm acc}$, assuming an electron energy of 10 TeV. The horizontal dotted line marks an acceleration time of one day, the maximum acceleration time of the 10 TeV electrons in the system from these observations. The vertical lines marked $B_{\rm apastron}$ and $B_{\rm periastron}$ mark the upper limits on the magnetic field strength at apastron and periastron respectively (these limits are independent of $\eta_{\rm acc}$). The shaded regions show the allowed regions of the parameter space for the system at apastron and periastron.

reduction in size of the pulsar wind termination shock could allow for increased acceleration efficiency on the timescale of a few hours, depending on the size and density of the disc fragments. Such a scenario could account for the exceptionally bright TeV flares and orbit-to-orbit variations seen in LS I +61° 303.

This research is supported by grants from the U.S. Department of Energy Office of Science, the U.S. National Science Foundation and the Smithsonian Institution, and by NSERC in Canada. We acknowledge the excellent work of the technical support staff at the Fred Lawrence Whipple Observatory and at the collaborating institutions in the construction and operation of the instrument. The VERITAS Collaboration is grateful to Trevor Weekes for his seminal contributions and leadership in the field of VHE gamma-ray astrophysics, which made this study possible. A. O'FdB acknowledges support through the Young Investigators Program of the Helmholtz Association. A.W. Smith acknowledges support from the Fermi Cycle 7 Guest Investigator Program, grant number NNH13ZDA001N.

REFERENCES

Abdo, A., et al. 2009, ApJ, 701, L123

Abdo, A. A., et al. 2010, ApJ, 722, 520

Abramowski, A., Aharonian, F., Ait Benkhali, F., et al. 2015, ArXiv e-prints, arXiv:1503.02711

Acciari, V., et al. 2008, ApJ, 679, 1427

Acciari, V. A., Aliu, E., Arlen, T., et al. 2009, ApJ, 698, L94

Aharonian, F., Akhperjanian, A. G., Aye, K.-M., et al. 2005a, A&A, 442, 1

—. 2005b, Science, 309, 746

Albert, J., et al. 2006, Science, 312, 1771

Aleksic, J., et al. 2012, ApJ, 746, 80

Aliu, E., Archambault, S., Behera, B., et al. 2013, ApJ, 779, 88

Aragona, C., et al. 2009, ApJ, 698, 514

Casares, J., et al. 2005, MNRAS, 360, 1105

Dhawan, V., et al. 2006, in Proc. of Microquasars and Beyond:From Binaries to Galaxies, in Proceedings of Science, Como, IT, ed. T. Belloni, p.52

Dubus, G. 2013, A&A Rev., 21, 64

Esposito, P., Caraveo, P. A., Pellizzoni, A., et al. 2007, A&A, 474, 575

Frail, D. A., & Hjellming, R. M. 1991, AJ, 101, 2126

Holder, J. 2015, The Astronomer's Telegram, 6785

Holder, J., et al. 2008, American Institute of Physics Conference Series, 1085, 657

Hutchings, J., & Crampton, D. 1981, PASP, 93, 486

Khangulyan, D., Aharonian, F., & Bosch-Ramon, V. 2008, MNRAS, 383, 467

Kieda, D. 2013, in Proceedings of the 33rd International Cosmic Ray Conference (ICRC2013)

Li, J., et al. 2012, ApJ, 744, L13

Li, T.-P., & Ma, Y.-Q. 1983, The Astrophysical Journal, 272, 317

Massi, M., & Jaron, F. 2013, A&A, 554, A105

Massi, M., Jaron, F., & Hovatta, T. 2015, A&A, 575, L9

Massi, M., et al. 2001, A&A, 376, 217

Paredes-Fortuny, X., Bosch-Ramon, V., Perucho, M., & Rib, M. 2015, A&A, 574, A77

Rolke, W. A., López, A. M., & Conrad, J. 2005, Nuclear Instruments and Methods in Physics Research A, 551, 493

This 2-column preprint was prepared with the AAS LaTeX macros v5.2.